IVYSPRING
INTERNATIONAL PUBLISHER

Theranostics

Research Paper

A pH-Responsive Host-guest Nanosystem Loading Succinobucol Suppresses Lung Metastasis of Breast Cancer

Zhaoling Dan[1,2,#], Haiqiang Cao[1,#], Xinyu He[1], Zhiwen Zhang[1,✉], Lili Zou[2], Lijuan Zeng[3], Yan Xu[2], Qi Yin[1], Minghua Xu[1], Dafang Zhong[1], Haijun Yu[1], Qi Shen[2], Pengcheng Zhang[1], Yaping Li[1,✉]

1. State key Laboratory of Drug Research & Center of Pharmaceutics, Shanghai Institute of Materia Medica, Chinese Academy of Sciences, Shanghai 201203, China.
2. School of Pharmacy, Shanghai Jiaotong University, Shanghai 200240, China
3. School of Pharmacy, Shenyang Pharmaceutical University, Shenyang, 110016, China.

#These authors contributed equally.

✉ Corresponding authors: Prof. Zhiwen Zhang (zwzhang0125@simm.ac.cn) and Prof. Yaping Li (ypli@simm.ac.cn) Tel/Fax: +86-21-2023-1979.

Abstract

Cancer metastasis is the leading reason for the high mortality of breast cancer. Herein, we report on a pH-responsive host-guest nanosystem of succinobucol (PHN) with pH-stimuli controlled drug release behavior to improve the therapeutic efficacy on lung metastasis of breast cancer. PHN was composed of the host polymer of β-cyclodextrin linked with multiple arms of N,N-diisopropylethylenediamine (βCD-DPA), the guest polymer of adamantyl end-capped methoxy poly(ethylene glycol) (mPEG-Ad), and the active agent of succinobucol. PHN comprises nanometer-sized homogenous spherical particles, and exhibits specific and rapid drug release in response to the intracellular acidic pH-stimuli. Then, the anti-metastatic efficacy of PHN is measured in metastatic 4T1 breast cancer cells, which effectively confirms the superior inhibitory effects on cell migration and invasion activities, VCAM-1 expression and cell-cell binding of RAW 264.7 to 4T1 cells. Moreover, PHN can be specifically delivered to the sites of metastatic nodules in lungs, and result in an obviously improved therapeutic efficacy on lung metastasis of breast cancer. Thereby, the pH-responsive host-guest nanosystem can be a promising drug delivery platform for effective treatment of cancer metastasis.

Key words: Host-guest nanosystem; pH-responsive; Cyclodextrin; Cancer metastasis; Breast cancer.

Introduction

Caner metastasis accounts for the high mortality of breast cancer [1, 2]. In clinic, breast cancer cells are preferentially invaded to distant organs of lung, liver, bone and brain [1, 3], in which 60-70% of patients who eventually died from breast cancer have metastases in their lungs. Despite the recent progress in new therapeutic agents and combinational regimens, the therapeutic efficacy in patients with metastatic disease is still limited with the five-year survival rate of only about 20% [1-6]. Actually, due to the complicated and abnormal microenvironments in cancer metastasis, many current therapies are not reaching the sites of the metastases, thereby leading to the limited therapeutic efficacy [3]. Thereby, it is of great necessity to find new approaches with efficient drug delivery to improve the therapeutic efficacy on cancer metastasis.

Supramolecular host-guest assembly offers a powerful and feasible platform for creation of nanosystems with desired properties and functionalities [7-14]. The host-guest nanosystem is based on the inherent noncovalent interactions between host and guest molecules, in which the β-cyclodextrin (β-CD)

and adamantine (Ad) molecules constitute the most common pair of host and guest molecules with high affinity [15-18]. Both β-CD and Ad can be modified with preferential functionalities to develop host-guest nanosystems, which demonstrate great potential for on-demand active drug delivery and cancer therapy [9, 19-22]. The cyclodextrin-based host-guest nanosystems can provide a fantastic drug delivery platform, but their applications in treating cancer metastasis have not been exploited yet.

The rapid and specific drug release from nanosystems in response to the abnormal tumor microenvironments can be of great interest to improve the therapeutic efficacy or diagnosis of cancer [23]. At the cellular level, the endocytic organelles of endosomes (pH ~5-6) or lysosomes (pH, ~4-5) exhibit sharp pH variation, which can be utilized to motivate the on-demand drug release behavior in response to the intracellular acidic environments [23-26]. The pH-responsive drug release can be achieved by de-
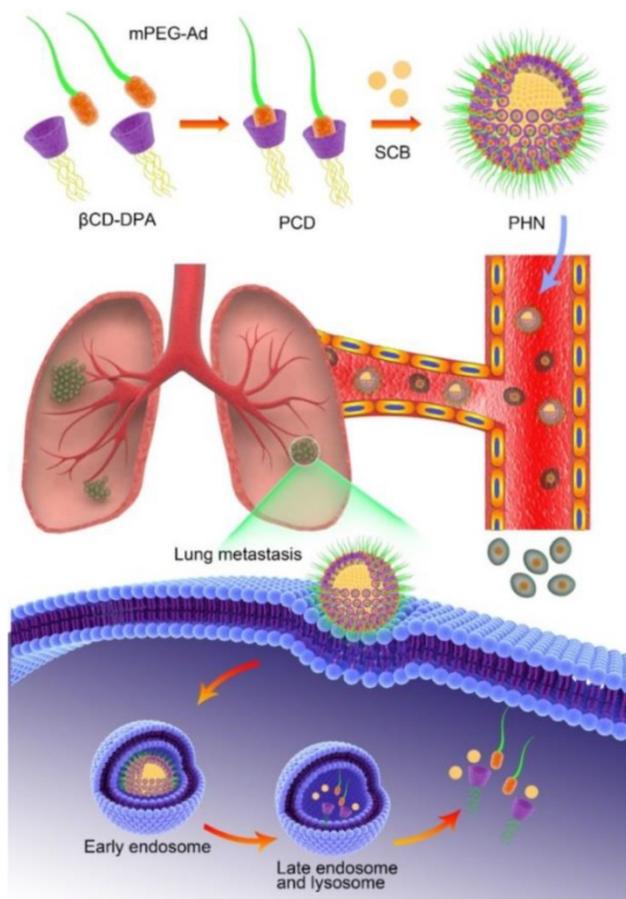

Scheme 1. Conceptual illustration of PHN mediated pH-responsive drug delivery to suppress the lung metastasis of breast cancer. The βCD-DPA and mPEG-Ad can be integrated into the supramolecular pseudo-diblock polymer of PCD via host-guest interactions, and then be assembled with lipophilic SCB into the nanosystem of PHN for targeted drug delivery to the metastatic nodules in lungs. After internalization into cancer cells, PHN can be disassociated with rapid and specific drug release in response to the intracellular acidic environments in late endosomes or lysosomes, thereby enhancing its therapeutic efficacy on cancer metastasis.

stabilization of the nanosystems or by degradation of the acid-liable linker that conjugated to the polymer backbone [27-30], thereby facilitating their pharmacological activities to achieve the anti-metastatic efficacy.

Herein, we put forward a pH-responsive host-guest nanosystem loading succinobucol (PHN) to suppress the lung metastasis of breast cancer. The delivery system of PHN is composed of one host polymer, one guest polymer and the active agent of succinobucol (Scheme 1). The host polymer is the β-CD molecules grafted with multiple arms of N,N-diisopropylethylenediamine (DPA) (βCD-DPA). Meanwhile, the guest polymer is Ad end capped methoxy poly(ethylene glycol) (mPEG-Ad). Succinobucol (SCB), a potent and selective inhibitor of VCAM-1, is supposed to be a potential candidate for inhibiting lung metastasis of breast cancer [31]. In this system, the hydrophobic βCD-DPA and hydrophilic mPEG-Ad can be integrated into amphiphilic supramolecular polymer of βCD-DPA/mPEG-Ad (PCD) due to the intermolecular host-guest interactions, and then be self-assembled with SCB into PHN (Scheme 1). Therein, the hydrophilic PEG segments of amphiphilic PCD polymer was used to form the outer shell of PHN nanoparticles, while the hydrophobic βCD-DPA segments could form the inner core of PHN to entrap the water-insoluble SCB with pH-stimuli responsive capability. In the intracellular acidic compartments, the hydrophobic DPA units in βCD-DPA can become hydrophilic due to the protonation of tertiary amino groups, thereby leading to the destabilization of PHN and rapid release of payload SCB to perform their pharmacological activities on cancer metastasis (Scheme 1). The formation of PHN and its pH-responsive properties are determined by in vitro characterizations. Then, the anti-metastatic efficacy is evaluated by in vitro and in vivo measurements to validate the effectiveness of PHN on inhibiting lung metastasis of breast cancer.

2. Experimental Sections

2.1 Materials

The DPA segments were first conjugated to β-CD to form the pH-responsive star-shaped βCD-DPA polymer, while the mPEG-Ad was synthesized as previously described method [32, 33]. The supramolecular pseudo-diblock polymer of βCD-DPA/mPEG-Ad (PCD) was formed by mixing the host and guest polymer at 1:1 molar ratio, and then determined by 2D NOSEY NMR spectroscopy. The detailed procedure and characterization were depicted in the supporting information. The critical aggregation concentration of PCD was determined by

the pyrene fluorescence probe spectrometry. Other materials including chemicals, reagents, cells and animals were also described in the supporting information.

2.2 Preparation and characterization of PHN

PHN was prepared by a self-assembly technique. Briefly, βCD-DPA and mPEG-Ad (1:1, molar ratio) was accurately weighted, dissolved in 50 μL of methanol and sonicated for 30 min. Then, 50 μL of SCB solution was added to the solution, and mixed by sonication. Then, the mixed solution was diluted with 900 μL of distilled water, and dialyzed against water to remove the methanol. The terminal concentration of SCB in PHN was about 4.0 mg/mL.

The morphology of PHN was observed under transmission electronic microscope (TEM) (JEOL JEM-2100F, Japan). Samples were negatively stained with phosphotungstic acid solution (1%, w/v) for the measurements. Meanwhile, the size distribution of PHN was determined on an instrument of Nano ZS 90 (Malvern, UK). Then, free SCB in PHN was separated by centrifugation method, and the drug amount in PHN was quantified by HPLC analysis to calculate the encapsulation efficiency and the drug loading capacity of PHN.

Then, to determine the dissociation of PHN at endosomal acidic environment, PHN was respectively diluted with PBS with pH 5.8 and pH 5.2. SCB was extremely insoluble in water, and easily precipitated in PBS when it was released from PHN. Samples were centrifuged at 3,500 g for 5 min, and the supernatant was observed under TEM to detect the morphology changes of PHN. Then, the in vitro release profiles of PHN were measured at 37 °C in PBS solution with various pH values from pH 7.4 to pH 5.2. Briefly, 100 μL PHN was respectively diluted into 900 μL of PBS at different pH values, mixed by vortex, and shaken at 100 rpm in a thermostatic oscillator (HZ-9611k, Hualida, China) at 37 °C. At predetermined time intervals, samples were centrifuged at 3,500 g for 5 min to remove the drug precipitation, and the drug amount in the supernatant was determined by HPLC analysis.

2.3 Cell cytotoxicity

The cytotoxicity of PHN was determined in the metastatic 4T1 breast cancer cells. Cells were added to 96-well plates at 6×10^3 cells/well and cultured overnight. Then, PHN, SCB and the PCD polymer (equivalent concentration to SCB) were respectively added to each well with SCB concentrations ranging from 4 ng/mL to 40 μg/mL. Cells without any treatment were performed as negative control. Thereafter, cells were incubated for further 48 h, and the cell viability

was measured by MTT assay method (Enspire, Perkin-Elmer, Singapore).

2.4 Cell apoptosis

To detect whether PHN could impact the cell viability, the cell populations in live cells, dead cells, at early apoptotic and late apoptotic stages were analyzed by FACS analysis. Cells were seeded into 12-well plates and cultured overnight for the attachment. Then, PHN and SCB were respectively incubated with cells at 400 ng/mL SCB for 48 h, and stained with the Annexin V-FITC/PI Apoptosis Detection kit (Invitrogen, USA). Cells without any treatment were performed as negative control. Samples were determined by the FACSCalibur system (BD, USA) to calculate the cell population percentages at each stage.

2.5 Cellular uptake

The cellular uptake of PHN in 4T1 cells were visualized under LCSM (Fluoview™ FV 1000, Olympus, Japan). Cells were seeded onto the round glass coverslips (Ø 10 mm) in 24-well culture plate at 1×10^4 cells/well and cultured overnight. The nile red labeled PHN was incubated with 4T1 cells for 2.0 h. Then, cells were respectively stained with LysoTracker Green DND-26 (Molecular Probe, USA) and Hoechst 33342 for visualization under LCSM. The uptake of PHN in 4T1 cells was denoted as the red fluorescence signals.

2.6 Inhibition of cell migration and cell invasion

The in vitro anti-metastatic efficacy of PHN was measured in the metastatic 4T1 cells by transwell mediated cell migration and invasion assays. For the migration assay, 1×10^5 cells was suspended in 100 μL of serum-free media, and added into the upper chamber of transwell inserts (pore size, 8 μm, Costar, USA) in 24-well plates. Meanwhile, for the invasion assay, 2.5×10^5 cells in 100 μL of serum-free media were added to the top chamber of Matrigel coated transwells inserts (BD, Bioscience). Then, 600 μL of culture media with 10% FBS was added to the lower chambers as chemoattractive agents. PHN and SCB were respectively added to both the upper and lower chambers at 400 ng/mL of SCB, and incubated for 24 h. The migrated or invaded cells were stained with crystal violet, photographed and further counted for the quantification.

2.7 Inhibition of VCAM-1 expression

To determine the inhibition effects of PHN on VCAM-1 expression on 4T1 cells, the VCAM-1 expression was determined by immunofluorescence assay and western-blot analysis. Cells were seeded to 24-well plates at 5×10^4 cells/well, cultured overnight,

and then incubated with PHN or SCB at 400 ng/mL of SCB for 48 h. Cells without any treatment were performed as negative control. For the immunofluorescence assay, cells were fixed, treated with the primary antibody (Ab19569, Abcam, UK) and Cy3 labeled secondary antibody (Beyotime, Jiangsu, China) according to the manufacturer's protocols. By contrast, the nuclei were stained with DAPI as control. The VCAM-1 expression was evidenced as red fluorescence signals under LCSM. Moreover, cells were lysed and the VCAM-1 content in the cell lysate was determined by western-blot analysis as previous described method [31].

2.8 Inhibiting cell-cell binding of RAW 264.7 to 4T1 cells

The 4T1 cells were seeded into 12-well plates at 1.5×10^5 cells/well, cultured overnight and incubated with SCB and PHN (400 ng/mL of SCB) for 48 h. Then, cells were labeled with Hoechst 33342 (5 µg/mL) for the binding assay. Meanwhile, RAW 264.7 cells were stained with DiI (red fluorescence) for 1 h, rinsed and harvested in PBS (pH 7.4). Then, RAW 264.7 cells (5.0 $\times 10^5$ cells in 1.0 ml PBS) were incubated with 4T1 cells for 30 min. The unbonded cells were removed, and the binding of RAW cells (red fluorescence) to 4T1 cells (blue fluorescence) were detected under fluorescence microscopy (IX81, Olympus, Japan). The cell-cell binding ratio was calculated as red counts compared to blue ones [31, 34].

2.9 In vivo behavior of PHN

The in vivo distribution profiles of PHN were evaluated in lung metastatic breast cancer models. The 4T1-luc cells were used to develop the lung metastatic breast cancer model. At 12 day after the inoculation, the formation of lung metastases was determined by in vivo bioluminescence assay (IVIS Spectrum, Perkin-Elmer) after intraperitoneal injection of luciferin (150 mg/kg). PHN was labeled with the near infrared probe of indocyanine green (ICG) by physical entrapments for the observations. Mice were given with the ICG labeled PHN via tail injection, and sacrificed at 2.0 h after the administration. Then, various major organs were carefully removed and imaged under the in vivo imaging system (IVIS Spectrum, Perkin-Elmer). The fluorescent signals were quantified by the accompanied software. Moreover, the specific delivery of PHN to the site of metastases was further determined by the in vivo multi-modal Spectrum/CT system (Perkin-Elmer, USA). In addition, the pharmacokinetic profiles of PHN and SCB was measured in rats after intravenous administration (40mg/kg) (n=4). To avoid the precipitation of water-insoluble SCB in the measurements, SCB was dissolved in the mixed solution of Solutol HS-15/dimethylacetamide (1:1, v/v) (40 mg/mL) and diluted with saline for the injection. The plasma concentration of SCB was determined by HPLC analysis as previous described methods [31].

2.10 In vivo therapeutic efficacy on inhibiting the lung metastasis of breast cancer

Mice were injected with 2×10^5 4T1-luc cells per mouse to generate the lung metastatic breast cancer model[31, 34]. After the inoculation, mice were divided into three groups (n=4), and respectively treated with saline, SCB solution and PHN (40mg/kg) by tail injection every three days. At day 12, the formation of lung metastasis was determined by *in vivo* bioluminescence measurements (IVIS Spectrum, Perkin-Elmer). Then, mice were autopsied and the lung tissues were removed. In each lung tissue, the visually detected metastatic nodules were counted. The inhibition of lung metastasis was calculated as the average metastatic nodules in PHN or SCB group compared to that in saline group. Moreover, the histological examination was performed by H&E staining to detect the metastatic foci in the lungs.

3. Results and Discussion

3.1 Formation of PHN and its pH-responsive properties

PHN was fabricated from the host βCD-DPA, guest mPEG-Ad and active agents of SCB. Therein, the host polymer of βCD-DPA was firstly synthesized by grafting DPA monomer to β-CD molecule to develop the star-shaped hydrophobic derivative with particular pH-responsive properties (Supporting information, Figure S1-3). It was determined that there are 6 arms of DPA linked the β-CD molecules. Meanwhile, adamantane methylamine was combined with mPEG-COOH (MW, 5000Da) to form the guest polymer of mPEG-Ad (Supporting information, Figure S4). The details of the synthesis procedure and NMR spectroscopic characterization were described in the Supporting Information (Supporting information, Figure S1-4). The hydrophobic βCD-DPA and hydrophilic mPEG-Ad could be merged into the amphiphilic supramolecular pseudo-diblock polymer of βCD-DPA/mPEG-Ad (PCD), which was formed by mixing them at molar ratio of 1:1 (Figure 1A). The formation of PCD was confirmed by 2D NOSEY NMR spectroscopy (Figure 1B). The NOE cross peaks between the inner protons of H(3) and H(5) of β-CD and those of Ad were readily detected, which suggested the inclusion of Ad moieties into the hydrophobic cavity of β-CD to form PCD via the host-guest interactions. The critical aggregation concentration of the

amphiphilic PCD was 1.23 µg/mL (Figure S5). Then, the amphiphilic PCD and water-insoluble SCB were self-assembled into the nanosystem of PHN, which was determined by TEM and dynamic light scattering (DLS) analysis (Figure 1C and D). The measured results indicated that PHN comprised homogeneous nanometer-sized spherical particles with the mean diameter of 110.0±40.36 nm and the polydispersity index (PDI) of 0.156 (Figure 1C and D). When PHN was diluted with distilled water to 100 times, the mean diameter of PHN was 105.2±39.47 nm with the PDI of 0.186. After 24 h, the mean diameter was 116.6±41.22 nm with the PDI of 0.218. These results indicated the good stability of PHN upon dilution as well as time alteration. Moreover, the drug loading capacity of SCB in PHN was 15.40±0.01% and the encapsulation efficiency was 95.65±0.02 %. Thereby, the water-insoluble SCB could be entrapped into the hydrophobic core of PHN due to its strong interactions with the hydrophobic parts of PCD.
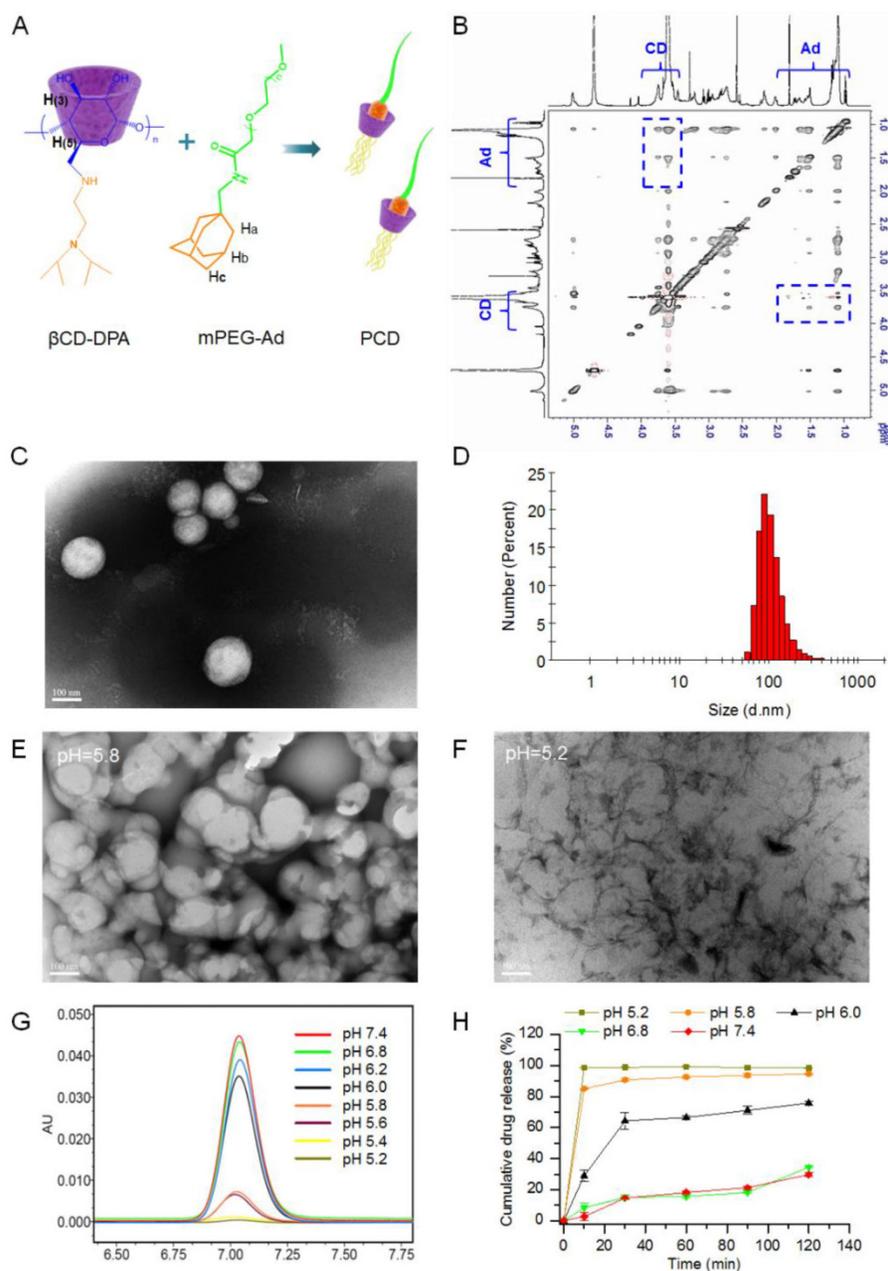

Figure 1. The formation and in vitro characterization of PHN. (A) The formation of βCD-DPA/mPEG-Ad supramolecular polymer (PCD) mediated by host-guest interactions between CD and Ad moieties; (B) the 2D NOSEY NMR spectrum of PCD; (C) typical TEM images of PHN at pH 7.4, scale bar = 100 nm; (D) the particle size distribution of PHN; (E) The typical TEM images of PHN at pH 5.8, scale bar = 100 nm; (F) the typical TEM images of PHN at pH 5.2, scale bar = 100 nm; (G) HPLC spectrum of pH-responsive drug release of PHN from pH 7.4 to pH 5.2; (H) the in vitro release profiles of PHN in PBS at different pH values.

It has been identified that the pH-responsive nanosystem could enable the on-demand drug release by virtue of the intracellular acidic environments to improve the therapeutic efficacy [35-40]. In the design of PHN, the hydrophobic βCD-DPA could become hydrophilic in the acidic endocytic organelles due to the protonation of tertiary amino groups in DPA [41], which could trigger the disassembly of PHN structure and specific drug release in response to the intracellular acidic pH-stimuli inside the cancer cells (Figure S6). To determine the pH-responsive properties, PHN was incubated with phosphate buffered solutions (PBS) at different pH values. Once the typical structure of PHN was dissociated or SCB was released from PHN, SCB would be largely precipitated in PBS due to the extreme water-insoluble property. At first, the morphology of PHN at lower pH values was analyzed by TEM measurements (Figure 1E and F). When PHN was diluted with PBS at pH 5.8, some drug precipitation was observable and the TEM images of the supernatant showed the typical structure of PHN collapsed in comparison with that of PHN at pH 7.4 (Figure 1C and E). Then, when PHN was incubated with PBS at pH 5.2, plenty of drug precipitation was readily detected and the TEM observations of the supernatant presented no typical structure of PHN (Figure 1F). Thereby, these TEM measurements directly displayed the disassociation of PHN at acidic environments, suggesting the specific and sensitive pH-responsive ability of PHN.

Then, the in vitro drug release of SCB from PHN at different pH values was quantified by high performance liquid chromatography (HPLC) (Figure 1G and H). PHN was incubated with series of PBS from pH 7.4 to pH 5.2 at 37 °C. At certain time intervals, samples were centrifuged and the drug amount in the supernatant was measured by HPLC analysis. The measured results indicated that a burst drug release from PHN when the pH values was lowered from 6.0 to 5.8, which denoted the specific and intelligent drug release in response to the endosomal acidic pH stimuli (Figure 1G). Furthermore, the in vitro release profiles of SCB from PHN were measured in PBS with different pH values to evaluate its pH-sensitivity to the extracellular and intracellular environments (Figure 1H). With the prolongation of time, the cumulative release of SCB was slowly increased at pH 7.4 and pH 6.8, and moderately raised to the maximum within 30 min at pH 6.0, but exhibited a sharp increase within 10 min to the maximum at pH 5.8 and 5.2. Typically, the cumulative drug release of PHN within 2 h was over 90% at pH 5.8 and 5.2, and 75% at pH 6.0, which was much higher than that at pH 6.8 and pH 7.4 (Figure 1H). These experimental results indicated that PHN could be stable in the extracellular pH environments, but present a specific and rapid drug release in response to the intracellular pH stimuli, which clearly verified the pH-responsive capability of PHN to the intracellular acidic microenvironments. The specific pH-stimuli motivated drug release from PHN could be appropriate for achieving the therapeutic efficacy on cancer metastasis.

3.2 In vitro cytotoxicity and anti-metastatic efficacy

To detect the in vitro anti-metastatic efficacy of PHN, experiments were performed in 4T1 metastatic breast cancer cells. The 4T1 cell line was a typical and commonly used lung metastatic cell line, which was originally derived from a mammary tumor that spontaneously emerged in Balb'c mice [34, 42]. At first, the in vitro cytotoxicity of PHN was measured to evaluate its effects on the cell viability (Figure 2). When the SCB concentration was less than 4 μg/mL, no obvious cytotoxicity was detected in SCB, PCD (equivalent dose to PHN) or PHN group, and no significant difference occurred among them (Figure 2A). Then, the cell populations in live cells, dead cells, at early apoptosis and late apoptosis stages were determined by FACS analysis (Figure 2B). At 400 ng/mL of SCB, the cell percentage in live cells was over 90%, which was comparable with that of the negative control. As a result, both SCB and PHN did not impact the cell viability of 4T1 cells at 400 ng/mL of SCB, which would hardly interfere with their anti-metastatic efficacy.

Then, the subcellular localization of PHN was observed under LCSM (Figure 2C). PHN was fluorescently labeled with hydrophobic dye of Nile red for the visualization. By contrast, the nuclei were stained with Hoechst 33342 (Blue, Beyotime), whereas the lysosomes was counterstained with LysoTracker Green DND-26 (Green, Molecular probe). A few yellow fluorescent signals (the combination of red and green fluorescence) were observed in 4T1 cells, which denoted the co-localization of PHN with the lysosomes after internalization (Figure 2C). Owing to the acidic environments in lysosomes (pH 4-5) and the pH-responsive properties of PHN, the localization of PHN in lysosomes could motivate the rapid and specific drug release in response to the pH stimuli, which could offer an essential opportunity to achieve the anti-metastatic efficacy.
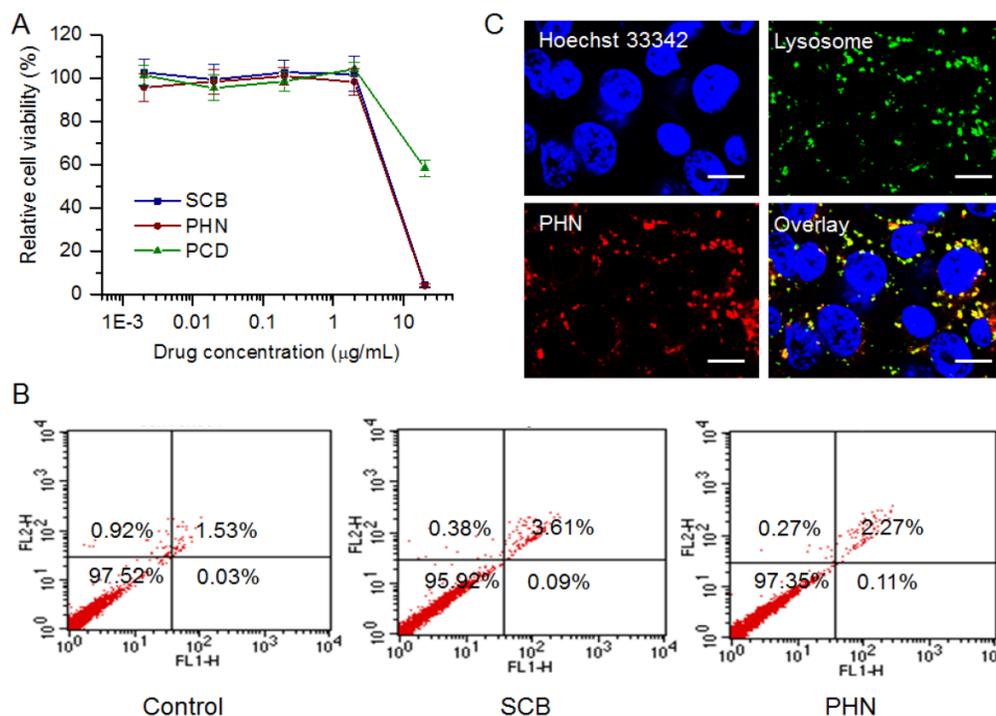
Figure 2. The in vitro evaluations of PHN on cell viability and its cellular uptake in metastatic 4T1 breast cancer cells. (A) The cytotoxicity of PHN, PCD (equivalent concentration to SCB) and SCB in 4T1 cells at series concentration of SCB; (B) the cell population percentages at each stage of 4T1 cells treated with SCB and PHN at 400 ng/mL of SCB measured by flow cytometry; (C) the subcellular localization of PHN with lysosomes in 4T1 cells under LCSM, scale bar = 10 μm.
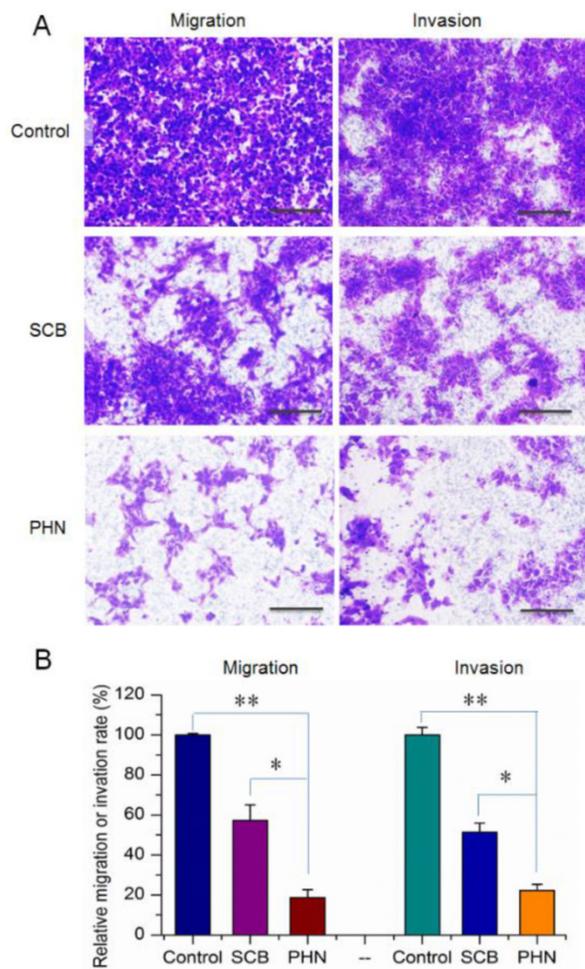

Figure 3. The in vitro inhibitory effects of PHN on cell migration and invasion activities of metastatic 4T1 cells. (A) The inhibition of cell migration and invasion of 4T1 cells treated with SCB and PHN at 400 ng/mL of SCB, scale bar=100 μm; (B) the quantified inhibition efficacy of PHN on cell migration and invasion activities, *$p<0.05$, **$p<0.01$.

Moreover, the cell migration and invasion activities of 4T1 cells were measured to determine the in vitro anti-metastatic efficacy of PHN (Figure 3). The migration and invasion abilities of cancer cells were directly related to their in vivo metastasis [43]. To know the inhibitory effects of PHN on the migration of 4T1 cells, experiments were performed by transwell mediated cell migration assays with 10% FBS as chemoattractive agents (Figure 3A and B). Compared to the negative control, the percentage of migrated cells was obviously reduced to 57.3% in SCB treated group, and further decreased to 18.7% with the PHN treatment (Figure 3). Similarly, in the cell invasion assays, the invaded cells across the Matrigel matrix coated transwell membrane in SCB treated group was 51.5% of the negative control, and further significantly reduced to 22.3% with the treatment of PHN (Figure 3). Moreover, significant difference was detected between PHN and SCB in inhibiting the cell migration and invasion activities (p<0.05) (Figure 3B). Typically, the inhibition rate of PHN on cell migration and invasion was respectively enhanced 1.9-fold and 1.6-fold than that of SCB group. Thereby, PHN presented a significant inhibition of cell migration and

invasion activities, which was much more effective than free SCB.

3.3 Inhibitory effects of PHN on VCAM-1 expression

VCAM-1 plays an essential role in the lung metastasis of breast cancer, which has been considered as a potential therapeutic target against cancer metastasis [34, 44]. SCB presents surprisingly potent and selective inhibitory activity on VCAM-1 expression, and has been identified as a promising candidate for treatment of lung metastasis [31]. The inhibitory effects of PHN on the VCAM-1 expression of 4T1 cells were first measured by immunofluorescence assay (Figure 4A). In the negative control, the VCAM-1 expression was denoted as red fluorescence and largely detected, which certificated the high expression of VCAM-1 expression on 4T1 cells. Then, the VCAM-1 expression was slightly reduced by SCB, and further obviously decreased with the treatment of PHN. Moreover, the VCAM-1 expression was determined by western-blot analysis (Figure 4B). The protein signals of VCAM-1 were readily detected in the negative control, then significantly reduced by SCB treatment, and further dramatically weakened in the presence of

PHN. Thereby, the VCAM-1 expression of 4T1 cells was notably inhibited by PHN.

Moreover, during the lung metastasis of breast cancer, the VCAM-1 on the surface of breast cancer cells could bind monocytes via the α4-integrin/VCAM-1 interactions, and facilitate the establishment of metastatic colonies in the lungs [34, 44]. The cell-cell binding of cancer cells to monocyte was a predominant aspect in the formation of lung metastatic nodules. The high expression of VCAM-1 on 4T1 cells have been identified above (Figure 4A and B). RAW 264.7 was a murine monocyte macrophage cell line that expressed α4-integrin [34], and was used for the cell-cell binding assay to evaluate the potential inhibitory effects of PHN. The 4T1 cancer cells were stained with Hoechst 33342 (blue fluorescence), while the RAW 264.7 cells were fluorescently labeled with a carbocyanine membrane probe of $DiIC_{18}$ (3) (DiI) (red fluorescence) (Figure 4C). The cell-cell binding of RAW 264.7 cells to 4T1 cancer cells was denoted as the binding ratio between red counts and blue ones. The binding ratio was 55.44% in the negative control, and greatly reduced to 9.18% and 2.88% with the treatment of SCB and PHN, respectively (Figure 4D).
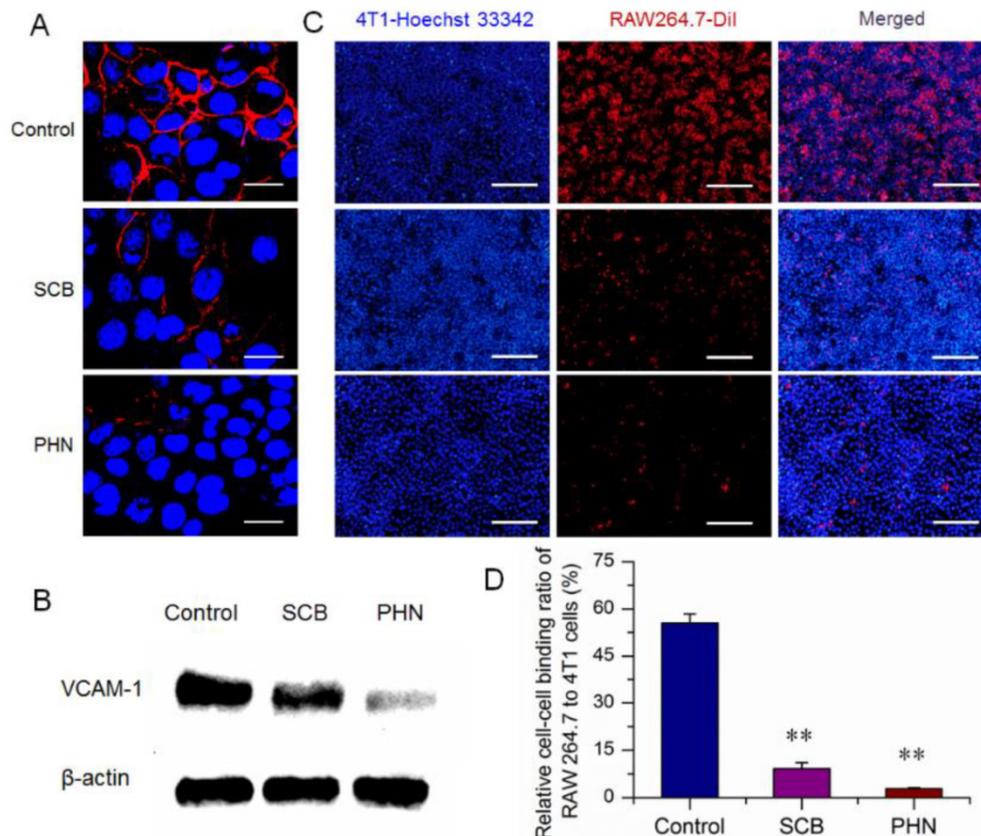

Figure 4. The in vitro inhibitory effect of PHN on VCAM-1 expression in 4T1 cells and cell-cell binding of RAW 264.7 to 4T1 cancer cells. (A) The VCAM-1 expression in 4T1 cells treated with SCB and PHN at 400 ng/mL of SCB, which was evidenced as red fluorescence, scale bar=10 μm; (B) the VCAM-1 expression in 4T1 cells determined by western-blot analysis; (C) the cell-cell binding of RAW 264.7 cells to 4T1 cells, in which 4T1 cancer cells were pretreated with SCB and PHN at 400 ng/mL of SCB, scale bar=100 μm; (D) the quantification of the binding ratio of RAW 264.7 cells to 4T1 cells, ** p<0.01.
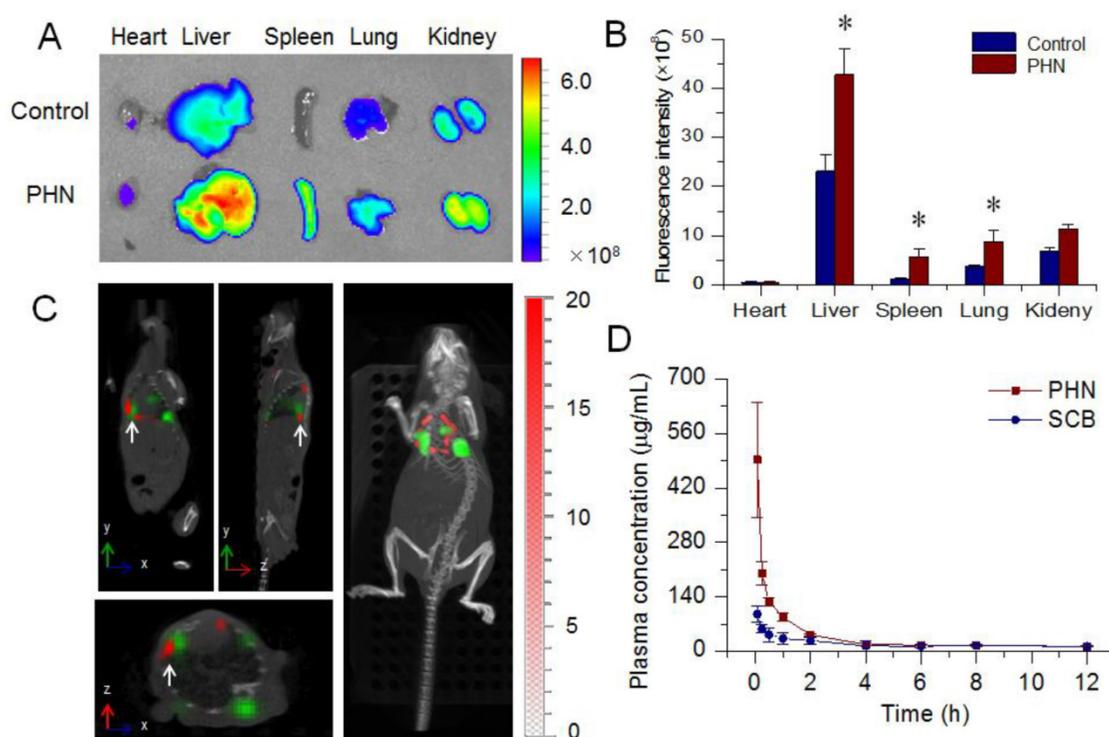
Figure 5. The in vivo behavior of PHN. (A) The ex vivo distribution of ICG labeled PHN in major organs of 4T1-luc induced lung metastatic breast cancer models; (B) the quantified distribution of PHN in major organs, *p< 0.05; (C) the specific targeting of PHN to metastatic nodules in 4T1-luc induced lung metastatic breast cancer models; (D) the in vivo pharmacokinetic profiles of PHN and SCB in rats after intravenous administration.

These experimental results indicated that the cell-cell binding of cancer cells to monocytes was effectively inhibited by PHN, which could result from the potential inhibition of VCAM-1 expression. Previous results indicated that the VCAM-1 depletion on breast cancer cells could significantly inhibit the formation of metastatic colonies in the lungs [34]. Accordingly, the remarkable inhibition of VCAM-1 expression and cell-cell binding of cancer cells to monocyte by PHN could be promising to reduce the incidence of lung metastases.

3.4 In vivo distribution and therapeutic efficacy on lung metastasis of breast cancer

The lung metastasis breast cancer model was induced by tail injection of 4T1-luc cells [34]. The formation of lung metastases was determined by in vivo bioluminescence assay (IVIS Spectrum, Perkin-Elmer) prior to the in vivo distribution assays. PHN was fluorescent labeled with ICG for the measurements under the in vivo imaging system (Figure 5A). The captured images indicated that the fluorescent signals of PHN in liver, spleen and lung were much higher than that of free ICG. Meanwhile, the quantified results showed that the mean fluorescence intensity from PHN was significantly enhanced by 2.33 folds in the lungs (Figure 5B). Moreover, the specific targeting of PHN to metastatic nodules was evaluated by in vivo multi-modal imaging system of

Spectrum/CT in a lung metastatic breast cancer model (Figure 5C). The fluorescent signals of PHN (red signals) can be specifically distributed in the site of metastatic nodules (green signals) (white arrows), which were also clearly identified in the reconstructed 3D movies. Thereby, PHN could induce a higher accumulation in lung tissues and be specifically delivered to the site of metastatic lesions in lungs. After reaching the metastatic nodules, PHN could be internalized into the cancer cells, and then dissociated to release the SCB in respond to the intracellular acidic environments in endosomes or lysosomes, which could be beneficial for inhibiting the lung metastasis of breast cancer. In addition, the pharmacokinetic profiles of PHN were investigated in rats after intravenous administration. Compared with the SCB solution, the plasma concentration of SCB from PHN was significantly higher than that of free SCB within two hours, and the area under concentration-time curve (AUC) was significantly increased by 1.77-fold (Figure 5D).

Then, the therapeutic efficacy of PHN was further validated in the lung metastatic breast cancer model. During the treatment, the body weight was hardly changed in mice of saline, SCB and PHN group (Figure S7). At the end, the lung metastasis was detected by in vivo bioluminescence assay after intraperitoneal injection of luciferin. The captured images showed that the bioluminescence signals were largely

detected in all the mice of negative control and SCB group, but was detectable in only one of the four residual animals with lower intensity (Figure 6A). Moreover, the lung tissues were removed at the end point and the visually detected metastatic nodules was counted to evaluate the extent of lung metastasis (Figure 6B). The average number of metastatic nodules per lung was 26.5±5.0 in negative control and 22.8±9.4 in SCB group, respectively. However, in PHN treated group, the average number of metastatic nodules was significantly reduced to 8.0±1.0, which was only 30.2% of the negative control and 35.1% of SCB group (Figure 6C). Furthermore, the histological examination was performed by H&E staining to detect the metastasis lesions in lung tissues, which was evidenced by clusters of cells with darkly staining nuclei (Figure 6D). The metastatic lesions were obviously observed in negative control and SCB group, but seldom detected in PHN group. These experimental results clearly verified that the lung metastasis of breast cancer was effectively inhibited by PHN, but not obviously affected by SCB. The effectiveness of PHN on inhibiting the lung metastasis of breast cancer mainly ascribe to the obviously increased inhibitory effects on cell migration and invasion activities, significant reduction of VCAM-1 expression and cell-cell binding of monocytes to cancer cells, and higher accumulation in lung tissues. Moreover, the enhanced anti-metastatic efficacy of PHN over SCB could result from the nanometer-sized nanostructure

of PHN and the specific pH-stimuli controlled drug release in response to the intracellular acidic environments. Additionally, the systemic toxicity of PHN was evaluated by histological examination in mice after multiple intravenous administrations. The pathological changes were detected under light microscope to determine the damages induced by PHN. Compared with the negative control, the PHN treated group displayed negligible damages in these organs, indicating the good biocompatibility in mice after multiple dosing (Figure S8).

4. Conclusion

In summary, a pH-responsive nanosystem of PHN was successfully developed via the host-guest interactions with effective inhibition of lung metastasis of breast cancer. PHN comprised nanometer-sized spherical particles with the mean diameter of 110.0±40.36 nm, and exhibited specific and sensitive pH-stimuli responsive capability. The inhibitory effects of SCB on cell migration and invasion activities, VCAM-1 expression in 4T1 cells and cell-cell binding of RAW 264.7 to 4T1 cells were obviously enhanced after its assembly into PHN. In particular, in the lung metastatic breast cancer model, the therapeutic efficacy on lung metastasis of breast cancer was greatly improved by PHN. Thereby, PHN could provide a promising drug delivery platform for treating lung metastasis of breast cancer.
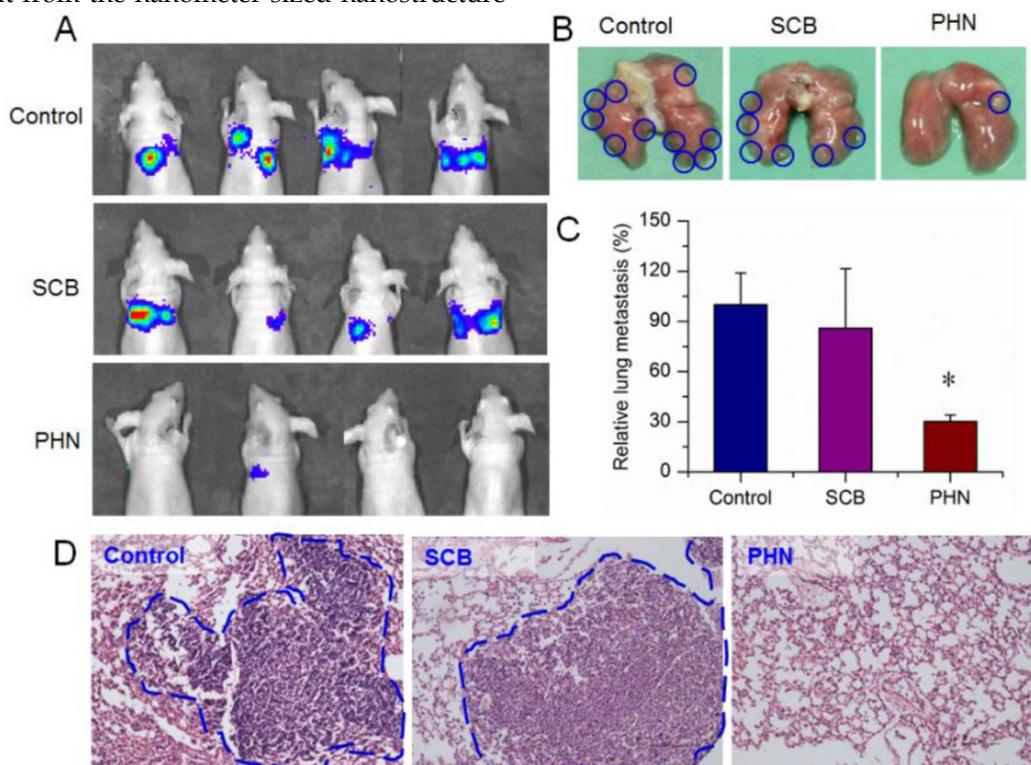

Figure 6. The in vivo therapeutic efficacy of PHN in lung metastatic breast cancer models treated with saline, SCB and PHN (n=4). (A) the in vivo bioluminescence imaging; (B) the typical lung tissues; (C) the average metastatic nodules per lung in mice, *p< 0.05; (D) the histological examination of metastatic foci in lung from each group.

Supplementary Material

Acknowledgements

Competing Interests

The authors have declared that no competing interest exists.

References

1. Eckhardt BL, Francis PA, Parker BS, Anderson RL. Strategies for the discovery and development of therapies for metastatic breast cancer. Nat. Rev. Drug Discov. 2012;11:479-97.
2. Fernandez Y, Cueva J, Palomo AG, Ramos M, de Juan A, Calvo L, et al. Novel therapeutic approaches to the treatment of metastatic breast cancer. Cancer Treat. Rev. 2010;36:33-42.
3. Schroeder A, Heller DA, Winslow MM, Dahlman JE, Pratt GW, Langer R, et al. Treating metastatic cancer with nanotechnology. Nat. Rev. Cancer. 2012;12:39-50.
4. Mi B, Yu C, Pan D, Yang M, Wan W, Niu G, et al. Pilot Prospective Evaluation of (18)F-Alfatide II for Detection of Skeletal Metastases. Theranostics. 2015;5:1115-21.
5. Lux J, White AG, Chan M, Anderson CJ, Almutairi A. Nanogels from metal-chelating crosslinkers as versatile platforms applied to copper-64 PET imaging of tumors and metastases. Theranostics. 2015;5:277-88.
6. Zhou Y, Shao G, Liu S. Monitoring Breast Tumor Lung Metastasis by U-SPECT-II/CT with an Integrin alpha(v)beta(3)-Targeted Radiotracer(99m)Tc-3P-RGD(2). Theranostics. 2012;2:577-88.
7. Wang L, Li LL, Fan YS, Wang H. Host-guest supramolecular nanosystems for cancer diagnostics and therapeutics. Adv. Mater. 2013;25:3888-98.
8. Zhang J, Ma PX. Cyclodextrin-based supramolecular systems for drug delivery: recent progress and future perspective. Adv.Drug Deliv. Rev. 2013;65:1215-33.
9. Hu QD, Tang GP, Chu PK. Cyclodextrin-based host-guest supramolecular nanoparticles for delivery: from design to applications. Accounts of chemical research. 2014;47:2017-25.
10. Dong R, Zhou Y, Huang X, Zhu X, Lu Y, Shen J. Functional supramolecular polymers for biomedical applications. Adv. Mater. 2015;27:498-526.
11. Zhao F, Yin H, Li J. Supramolecular self-assembly forming a multifunctional synergistic system for targeted co-delivery of gene and drug. Biomaterials. 2014;35:1050-62.
12. Jung H, Park KM, Yang JA, Oh EJ, Lee DW, Park K, et al. Theranostic systems assembled in situ on demand by host-guest chemistry. Biomaterials. 2011;32:7687-94.
13. Fan H, Hu QD, Xu FJ, Liang WQ, Tang GP, Yang WT. In vivo treatment of tumors using host-guest conjugated nanoparticles functionalized with doxorubicin and therapeutic gene pTRAIL. Biomaterials. 2012;33:1428-36.
14. Shen J, Kim HC, Su H, Wang F, Wolfram J, Kirui D, et al. Cyclodextrin and polyethylenimine functionalized mesoporous silica nanoparticles for delivery of siRNA cancer therapeutics. Theranostics. 2014;4:487-97.
15. Wen YT, Zhang ZX, Li J. Highly Efficient Multifunctional Supramolecular Gene Carrier System Self-Assembled from Redox-Sensitive and Zwitterionic Polymer Blocks. Adv. Funct. Mater. 2014;24:3874-84.
16. Harries D, Rau DC, Parsegian VA. Solutes probe hydration in specific association of cyclodextrin and adamantane. J. Am. Chem. Soc. 2005;127:2184-90.
17. Lai WF. Cyclodextrins in non-viral gene delivery. Biomaterials. 2014;35:401-11.
18. [18] Hu Y, Yuan W, Zhao NN, Ma J, Yang WT, Xu FJ. Supramolecular pseudo-block gene carriers based on bioreducible star polycations. Biomaterials. 2013;34:5411-22.
19. Dan Z, Cao H, He X, Zeng L, Zou L, Shen Q, et al. Biological stimuli-responsive cyclodextrin-based host-guest nanosystems for cancer therapy. Int. J. Pharm. 2015;483:63-8.
20. Namgung R, Mi Lee Y, Kim J, Jang Y, Lee BH, Kim IS, et al. Poly-cyclodextrin and poly-paclitaxel nano-assembly for anticancer therapy. Nat. Commun. 2014;5:3702.
21. Zhang J, Yuan ZF, Wang Y, Chen WH, Luo GF, Cheng SX, et al. Multifunctional envelope-type mesoporous silica nanoparticles for tumor-triggered targeting drug delivery. J. Am. Chem. Soc. 2013;135:5068-73.
22. Shi Q, Zhang L, Liu M, Zhang X, Zhang X, Xu X, et al. Reversion of multidrug resistance by a pH-responsive cyclodextrin-derived nanomedicine in drug resistant cancer cells. Biomaterials. 2015;67:169-82.
23. Mura S, Nicolas J, Couvreur P. Stimuli-responsive nanocarriers for drug delivery. Nat. Mater. 2013;12:991-1003.
24. Webb BA, Chimenti M, Jacobson MP, Barber DL. Dysregulated pH: a perfect storm for cancer progression. Nat. Rev. Cancer. 2011;11:671-7.
25. Torchilin VP. Multifunctional, stimuli-sensitive nanoparticulate systems for drug delivery. Nat. Rev. Drug Discov. 2014;13:813-27.
26. Huang G, Chen H, Dong Y, Luo X, Yu H, Moore Z, et al. Superparamagnetic iron oxide nanoparticles: amplifying ROS stress to improve anticancer drug efficacy. Theranostics. 2013;3:116-26.
27. Wang Y, Shim MS, Levinson NS, Sung H-W, Xia Y. Stimuli-Responsive Materials for Controlled Release of Theranostic Agents. Adv. Funct. Mater. 2014;24:4206-20.
28. Du Y, Chen W, Zheng M, Meng F, Zhong Z. pH-sensitive degradable chimaeric polymersomes for the intracellular release of doxorubicin hydrochloride. Biomaterials. 2012;33:7291-9.
29. Sharker SM, Lee JE, Kim SH, Jeong JH, In I, Lee H, et al. pH triggered in vivo photothermal therapy and fluorescence nanoplatform of cancer based on responsive polymer-indocyanine green integrated reduced graphene oxide. Biomaterials. 2015;61:229-38.
30. Tang S, Yin Q, Su J, Sun H, Meng Q, Chen Y, et al. Inhibition of metastasis and growth of breast cancer by pH-sensitive poly (β-amino ester) nanoparticles co-delivering two siRNA and paclitaxel. Biomaterials. 2015;48:1-15.
31. Cao H, Zhang Z, Zhao S, He X, Yu H, Yin Q, et al. Hydrophobic interaction mediating self-assembled nanoparticles of succinobucol suppress lung metastasis of breast cancer by inhibition of VCAM-1 expression. J. Control. Release. 2015;205:162-71.
32. Madhavan N, Robert EC, Gin MS. A highly active anion-selective aminocyclodextrin ion channel. Angew. Chem. Int. Ed. 2005;44:7584-7.
33. Bellocq NC, Pun SH, Jensen GS, Davis ME. Transferrin-containing, cyclodextrin polymer-based particles for tumor-targeted gene delivery. Bioconjug.Chem. 2003;14:1122-32.
34. Chen Q, Zhang XHF, Massague J. Macrophage Binding to Receptor VCAM-1 Transmits Survival Signals in Breast Cancer Cells that Invade the Lungs. Cancer Cell. 2011;20:538-49.
35. Li C, Xia J, Wei X, Yan H, Si Z, Ju S. pH-Activated Near-Infrared Fluorescence Nanoprobe Imaging Tumors by Sensing the Acidic Microenvironment. Adv. Funct. Mater. 2010;20:2222-30.
36. Colson YL, Grinstaff MW. Biologically Responsive Polymeric Nanoparticles for Drug Delivery. Adv. Mater. 2012;24:3878-86.
37. Li J, Qu X, Payne GF, Zhang C, Zhang Y, Li J, et al. Biospecific Self-Assembly of a Nanoparticle Coating for Targeted and Stimuli-Responsive Drug Delivery. Adv. Funct. Mater. 2015;25:1404-17.
38. Yu J, Deng H, Xie F, Chen W, Zhu B, Xu Q. The potential of pH-responsive PEG-hyperbranched polyacylhydrazone micelles for cancer therapy. Biomaterials. 2014;35:3132-44.
39. Chiang Y-T, Lo C-L. pH-Responsive polymer-liposomes for intracellular drug delivery and tumor extracellular matrix switched-on targeted cancer therapy. Biomaterials. 2014;35:5414-24.
40. Xiao Y, Hong H, Matson VZ, Javadi A, Xu W, Yang Y, et al. Gold Nanorods Conjugated with Doxorubicin and cRGD for Combined Anticancer Drug Delivery and PET Imaging. Theranostics. 2012;2:757-68.
41. Yu H, Zou Y, Wang Y, Huang X, Huang G, Sumer BD, et al. Overcoming endosomal barrier by amphotericin B-loaded dual pH-responsive PDMA-b-PDPA micelleplexes for siRNA delivery. ACS Nano. 2011;5:9246-55.
42. Zhang Z, Cao H, Jiang S, Liu Z, He X, Yu H, et al. Nanoassembly of probucol enables novel therapeutic efficacy in the suppression of lung metastasis of breast cancer. Small. 2014;10:4735-45.
43. Kramer N, Walzl A, Unger C, Rosner M, Krupitza G, Hengstschlager M, et al. In vitro cell migration and invasion assays. Mutation Res. 2013;752:10-24.
44. Chen Q, Massague J. Molecular Pathways: VCAM-1 as a Potential Therapeutic Target in Metastasis. Clin. Cancer Res. 2012;18:5520-5.